Collective dynamics near fluid phase transitions

Martin Schoen* and Fabien Porcheron†

Stranski-Laboratorium für Physikalische und Theoretische Chemie, Sekretariat TC 7, Fakultät für Mathematik und Naturwissenschaften, Technische Universität Berlin, Straße des 17. Juni 124, D-10623 Berlin, Germany

(Received 17 January 2003; published 27 May 2003)

By means of molecular dynamics simulations, we calculate the intermediate scattering function $F(k_\parallel,t)$ where $k_\parallel$ is the wave number and t is the time. We focus on thermodynamic states in the vicinity of a fluid phase transition in bulk and confined systems which we locate in parallel Monte Carlo simulations in the grand canonical ensemble. As one approaches the limit of stability of the fluid (i.e., its spinodal) from either low- or high-density branches of a subcritical isotherm, $F(k_\parallel,t)$ becomes increasingly long-range. The apparent lack of decorrelation in the metastable regime can be understood within the framework of a simple mean-field theory that links the long-range nature of $F(k_\parallel,t)$ to a divergence of the ratio of isostress and isochoric heat capacities γ. Our results suggest that as one approaches the spinodal the dynamic structure factor $S(k_\parallel,\omega)$ (ω frequency), which is related to $F(k_\parallel,t)$ through a Laplace transformation, should undergo a qualitative change from the usual triplet of Brillouin and Rayleigh lines to a singlet (δ-function-like peak) centered at $\omega=0$ for states directly at the spinodal. This qualitative change in $S(k_\parallel,\omega)$ should be measurable in scattering experiments thereby promoting more detailed insight into the phase behavior and thermodynamic stability of confined and bulk fluids.

DOI: 10.1103/PhysRevE.67.051202 PACS number(s): 68.55.−a, 62.10.+s, 61.46.+w, 62.25.+g

I. INTRODUCTION

In a recent publication, we investigated the collective dynamics of dense fluids in terms of the intermediate scattering function by means of equilibrium (i.e., microcanonical ensemble) molecular dynamics (MD) simulations [1]. We focused, in particular, on fluids confined by chemically homogeneous, planar substrates (nanoscopic slit pore) where the intermediate scattering function $F(k_\parallel,t)\propto\langle\rho(-\mathbf{k}_\parallel,0)\rho(\mathbf{k}_\parallel,t)\rangle$ can be expressed in terms of the time autocorrelation function of the Fourier components of the local density $\rho(\mathbf{k}_\parallel,t)$. Here, $\mathbf{k}_\parallel=(m/L,n/L)$ is the wave vector and t is time; m and n are integers and L denotes the length of the (square) computational cell in the x-y plane. Since we restrict the analysis to two-dimensional in-plane wave vectors, F depends only on the wave number $k_\parallel\equiv|\mathbf{k}_\parallel|$ because the confined fluid is homogeneous (and therefore its properties are translationally invariant) across the x-y plane parallel to the confining substrate surfaces. In other words, we consider only modes propagating in a direction parallel to the slit-pore walls.

This restriction permits us to develop a hydrodynamic theory for $F(k_\parallel,t)$ starting from z-averaged conservation laws for heat, mass, and momentum currents eventually leading to a closed expression for $F(k_\parallel,t)$ in terms of a set of material constants [1]. The resulting expression for $F(k_\parallel,t)$ is *formally* equivalent to $F(k,t)$ in the bulk where $k=|(l/L,m/L,n/L)|$ is the three-dimensional counterpart of $k_\parallel$, and l, m, and n are integers [2–4]. This reflects the higher symmetry of the bulk fluid compared with the confined one since the latter is exposed to a (z-dependent) external potential representing the pore walls.

Fitting the hydrodynamic expression for $F(k_\parallel,t)$ to MD data permits one to determine the set of material constants *in principle*. However, a number of additional assumptions are required to derive $F(k_\parallel,t)$ in the hydrodynamic regime [1]. Thus, the resulting expression is correct only to order $O(k_\parallel^2)$. Unfortunately, central processing unit (CPU)-time restrictions in the MD simulations do not permit one to make $k_\parallel$ small (i.e., L large) enough so that higher-order terms are negligible. Hence, the set of material constants obtained from the fit to the MD data depends on $k_\parallel$ (i.e., on L) in a nonanalytic form over the $k_\parallel$ range accessible. Any extrapolation to the infinite-system limit (i.e., $k_\parallel\to 0$) must be regarded unsafe and the values extracted from such an extrapolation potentially erroneous [2].

To obtain reliable estimates for the set of material constants determining $F(k_\parallel,t)$ in the hydrodynamic regime, we proposed an alternative approach based upon the memory function $M(k_\parallel,t)$. The memory function is related to $F(k_\parallel,t)$ through the Volterra integrodifferential equation that can be solved numerically for $M(k_\parallel,t)$ using the MD generated $F(k_\parallel,t)$ as input [1]. We also developed a limiting hydrodynamic expression for $M(k_\parallel,t)$ having the advantage that it is *exact* to all orders of $k_\parallel$ unlike $F(k_\parallel,t)$. Hence, analyzing the numerically obtained $M(k_\parallel,t)$ *via* this hydrodynamic form gives us the set of transport coefficients *independent* of $k_\parallel$ over a range of system sizes where MD simulations are still feasible employing nothing but standard simulation techniques [5].

Assuming certain inequalities to hold between the material constants, it is shown in Ref. [1] that $M(k_\parallel,t)$ should be a damped oscillatory function of time in the hydrodynamic regime as far as thermodynamically stable states are concerned. However, as we shall demonstrate in this paper, a significant change in $M(k_\parallel,t)$ is observed as one penetrates

*Electronic address: martin.schoen@fluids.tu-berlin.de

†Electronic address: fabien.porcheron@fluids.tu-berlin.de

into the regime of metastable thermodynamic states along a subcritical isotherm either from the low- or high-density side of the two-phase region. It turns out that $M(k_\parallel,t)\to 0$ irrespective of $k_\parallel$ and t as one approaches the stability limit of the (metastable) fluid phase. This change in the ''memory'' of density modes eventually enables us to locate the stability limit of fluids from a dynamical perspective.

Based upon the present results, we predict a qualitative change in the dynamic structure factor $S(k_\parallel,\omega)$, which is related to $F(k_\parallel,t)$ through a Laplace transformation. The former is frequently measured in light [6,7] or neutron scattering [8] experiments and should exhibit a change from the usual triplet of Brillouin and Rayleigh lines to a singlet centered at the frequency $\omega=0$ as one approaches the stability limit.

The remaining paper is organized as follows. In Sec. II, we introduce our model system. In Secs. III A and III B, we define $F(k_\parallel,t)$ and $M(k_\parallel,t)$. Section III C is devoted to the development of a mean-field theory that we employ to rationalize the results of our MD simulations. In Sec. III D, we summarize basic concepts of stability of thermodynamic phases and their relation to the quantities of interest in the context of this work. Important technical details are summarized in Sec. IV A. In Sec. IV B, we determine the stability limit of fluid phases and analyze confinement effects in Sec. IV C. The paper concludes with a summary and discussion of our findings in Sec. V.

II. THE MODEL

We consider N spherically symmetric molecules interacting in a pairwise fashion *via* the so-called shifted force potential [5]

$$u_{ff}(r)=\begin{cases} u_{\mathrm{LJ}}(r)-u_{\mathrm{LJ}}(r_c)+u'_{\mathrm{LJ}}(r_c)(r_c-r), & r\leqslant r_c \\ 0, & r>r_c, \end{cases} \tag{2.1}$$

where r is the distance between a pair of molecules, $u_{\mathrm{LJ}}(r)$ is given by

$$u_{\mathrm{LJ}}(r)=4\epsilon\left[\left(\frac{\sigma}{r}\right)^{12}-\left(\frac{\sigma}{r}\right)^{6}\right], \tag{2.2}$$

where ϵ is the depth of the attractive well, σ is the ''diameter,'' and $u'_{\mathrm{LJ}}(r_c)=du_{\mathrm{LJ}}(r)/dr|_{r=r_c}$. In the actual simulations, $r_c=2.5\sigma$ so that we are dealing with explicitly short-range interactions. Since the shifted-force potential and its first derivative go to zero continuously at $r=r_c$, corrections due to the finite cutoff radius r_c are not required for any of the quantities of interest. The fluid-substrate interaction is modeled according to the potential function

$$u_{fs}^{[k]}(z)=2\pi\rho_w\sigma^2\epsilon\left[\frac{2}{5}\left(\frac{\sigma}{s_z/2\pm z}\right)^{10}-\left(\frac{\sigma}{s_z/2\pm z}\right)^{4}\right], \tag{2.3}$$

where ''+'' refers to the lower substrate ($k=1$) located at $z_w=-s_z/2$ and ''−'' to the upper one ($k=2$) at $z_w=+s_z/2$. In Eq. (2.3), $\rho_w\sigma^2=0.79$ is the areal density of solid atoms forming the substrate planes [9]. Since $u_{fs}^{[k]}(z)$ depends only on the distance of a fluid molecule from the substrate planes, properties of the confined system are (on an average) translationally invariant across the x-y plane.

To follow the time evolution of our system, we solve Newton's equation numerically using the so-called velocity Verlet algorithm [5]. To integrate the equation of motion by this finite-difference scheme, a time step of $\delta t=4.63\times10^{-3}$ in the customary dimensionless (i.e., ''reduced'') units is used. Energy is then conserved to about 2×10^{-4} for a typical run of 10^5 time steps. Reduced units are also used for all other quantities of interest, which are summarized in Table 1 of Ref. [1].

III. THEORY

A. The intermediate scattering function

In Ref. [1], we showed that microscopically the intermediate scattering function for a fluid confined to a slit pore with chemically homogeneous substrate surfaces can be written as

$$F(k_\parallel,t)=S^{-1}(k_\parallel)\langle\rho(-\boldsymbol{k}_\parallel)\rho(\boldsymbol{k}_\parallel,t)\rangle, \tag{3.1}$$

where $\boldsymbol{k}_\parallel=(k_x,k_y)\in\mathbb{R}^2$ is a wave vector in reciprocal space. Here $S(k_\parallel)=\langle\rho(-\boldsymbol{k}_\parallel)\rho(\boldsymbol{k}_\parallel)\rangle$ is the static structure factor [10],

$$\rho(\boldsymbol{k}_\parallel,t)=\sum_{m=1}^{N}\exp[-i\boldsymbol{k}_\parallel\cdot\boldsymbol{R}_m(t)] \tag{3.2}$$

is the Fourier component of the local density, $\boldsymbol{R}_m$ is the position of particle m in the x-y plane, and $\rho(\boldsymbol{k}_\parallel)$ is shorthand notation for $\rho(\boldsymbol{k}_\parallel,0)$. The dependence of F on $k_\parallel=|\boldsymbol{k}_\parallel|$ reflects the translational invariance of system properties in the x-y plane.

Equation (3.1) may be Laplace transformed to give

$$\begin{aligned} F(k_\parallel,s)&=S(k_\parallel)^{-1}\langle\rho(-\boldsymbol{k}_\parallel)\rho(\boldsymbol{k}_\parallel,s)\rangle \\ &=\frac{(s+ak_\parallel^2)(s+b_\parallel k_\parallel^2)+(\gamma-1)v_\parallel^2k_\parallel^2/\gamma}{s(s+ak_\parallel^2)(s+b_\parallel k_\parallel^2)+sv_\parallel^2k_\parallel^2+(a/\gamma)v_\parallel^2k_\parallel^4}, \end{aligned} \tag{3.3}$$

where the second line follows from hydrodynamic considerations detailed in Ref. [1]. In Eq. (3.3), $a\equiv\lambda/\rho c_{As_z}$ (λ thermal conductivity and c_{As_z} isochoric heat capacity), $b_\parallel$ is the lateral kinematic viscosity, $\gamma\equiv c_{\tau_\parallel}/c_{As_z}$ ($c_{\tau_\parallel}$ heat capacity at constant transverse stress $\tau_\parallel$), and $v_\parallel$ is the adiabatic, in-plane velocity of sound. We may then transform $F(k_\parallel,s)$ back to the time domain following the procedure described in detail in Ref. [1] to get

$$\begin{aligned} F(k_\parallel,t)=\frac{\gamma-1}{\gamma}\exp(-D_Tk_\parallel^2t)+\frac{1}{\gamma}\exp(-\Gamma k_\parallel^2t)[\cos(v_\parallel k_\parallel t) \\ +d(k_\parallel)\sin(v_\parallel k_\parallel t)], \end{aligned} \tag{3.4}$$

where the thermal diffusivity is defined as

$$D_T \equiv \frac{a}{\gamma}, \tag{3.5}$$

the sound attenuation coefficient as

$$\Gamma \equiv \frac{1}{2}[D_T(\gamma-1)+b_\parallel], \tag{3.6}$$

and

$$d(k_\parallel) \equiv [\Gamma+(\gamma-1)D_T]\frac{k_\parallel}{v_\parallel}. \tag{3.7}$$

It is important to realize that the expression in the second line of Eq. (3.3) is *exact* in the hydrodynamic regime, whereas additional assumptions are required to obtain the equivalent expression in the time domain [see Eq. (3.4)]. In the hydrodynamic regime, the latter is therefore only *approximately* correct to order $O(k_\parallel^2)$ [1].

Unfortunately, in MD, a lower limit of $k_\parallel \propto L^{-1}$ exists below which $k_\parallel$ cannot be reduced easily because the size of the simulation cell cannot be made arbitrarily large. The latter is due to the CPU time required to simulate the temporal evolution of increasingly larger many-particle systems which becomes prohibitive sooner or later. Thus, if Eq. (3.4) is fitted to data generated in MD simulations *via* Eqs. (3.1) and (3.2) over the typical range of wave numbers $k_\parallel$ accessible, the set of coefficients $\{\gamma, v_\parallel, D_T, \Gamma\}$ turns out to depend on $k_\parallel$ even though excellent fits are usually obtained [see Figs. 1(a) and 2(a)]. Since, on the other hand, the dependence of $\{\gamma, v_\parallel, D_T, \Gamma\}$ on $k_\parallel$ is unknown analytically, an extrapolation of these quantities to the thermodynamic limit ($k_\parallel \to 0$ or equivalently $L \to \infty$, $N/As_z, s_z = \text{const}$, and $A = L^2$) is generally prohibited.

B. Memory function

A determination of $\{\gamma, v_\parallel, D_T, \Gamma\}$ in the hydrodynamic regime but *independent* of the size of the simulation system (i.e., independent of $k_\parallel$) is, however, possible following the recipe proposed in Ref. [1]. It is based on solving Volterra's equation

$$-\frac{dF(k_\parallel,t)}{dt} = \int_0^t dt' M(k_\parallel,t')F(k_\parallel,t-t'), \quad \forall\, k_\parallel \tag{3.8}$$

numerically for the memory kernel $M(k_\parallel,t)$ using as input $F(k_\parallel,t)$ from MD. This can be achieved by employing an algorithm suggested by Berne and Harp [11].

Equation (3.8) can also be Laplace transformed and then solved *analytically* for $M(k_\parallel,s)$ using also Eq. (3.3). The result can be transformed back into the time domain to give [1]

$$M(k_\parallel,t) = M_0(k_\parallel)\exp(-x't)[\cosh(ix''t) - iy''\sinh(ix''t)], \tag{3.9}$$

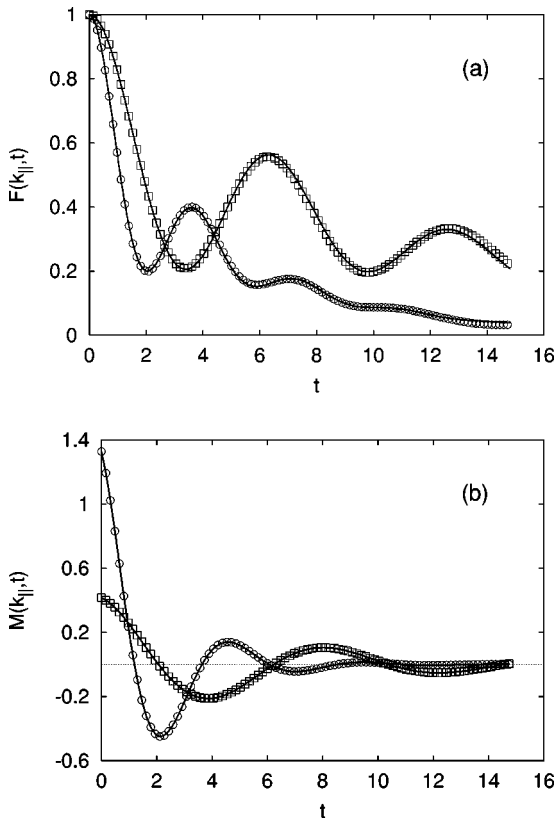

FIG. 1. (a) Intermediate scattering function $F(k_\parallel,t)$ as a function of time t for bulk fluid; (□) $k_\parallel = 0.22$, (○) $k_\parallel = 0.38$; the solid line is the fit of Eq. (3.4) to MD data. (b) as (a), but for $M(k_\parallel,t)$; the solid line is the fit of Eq. (3.11) to discrete data points.

where

$$M_0(k_\parallel) = \frac{v_\parallel^2 k_\parallel^2}{\gamma}, \tag{3.10a}$$

$$x' = \left(\Gamma + \frac{D_T}{2}\right)k_\parallel^2, \tag{3.10b}$$

$$x'' = v_\parallel k_\parallel \sqrt{\frac{\gamma-1}{\gamma} + O(k_\parallel^2)} \simeq v_\parallel k_\parallel \sqrt{\frac{\gamma-1}{\gamma}}, \tag{3.10c}$$

$$y'' = \sqrt{\frac{M_0(\gamma-1)}{x''^2} - 1} \simeq 0. \tag{3.10d}$$

At this point, it is important to realize that the backtransformation of the analytic expression for $M(k_\parallel,s)$ into the time domain does not require any additional simplifying assumptions like the ones invoked to get Eq. (3.4) from Eq. (3.3). Thus, unlike Eq. (3.4), Eq. (3.9) is *exact* to all orders in $k_\parallel$ in the hydrodynamic regime [1].

Since $x'' \in \mathbb{R}$, Eqs. (3.10c) and (3.10d) permit to simplify the expression given in Eq. (3.9) and rewrite it as

$$M(k_\parallel,t) = M_0(k_\parallel)\exp(-x't)\cos(x''t). \tag{3.11}$$

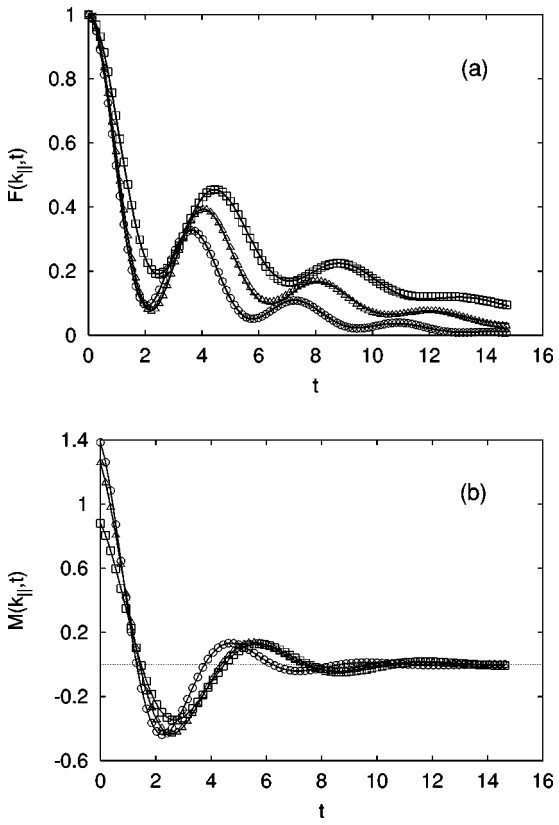

FIG. 2. (a) Intermediate scattering function $F(k_\parallel,t)$ as a function of time t for $k_\parallel=0.3142$; (□) bulk fluid, (△) confined fluid, $s_z=4.1$; (○) confined fluid, $s_z=1.9$. (b) as (a), but for $M(k_\parallel,t)$.

Parameters $\{M_0,x',x''\}$ can be determined by fitting Eq. (3.11) to the numerical solution of Eq. (3.8). As before, for $F(k_\parallel,t)$ an excellent representation of the MD-generated data is achieved [see Figs. 1(b) and 2(b)].

C. Mean-field theory

At this point, it seems worthwhile to briefly recall the hydrodynamic expression for $F(k_\parallel,t)$ [see Eq. (3.4)]. One realizes that among the four constants determining its functional form, two (i.e., γ and $v_\parallel$) play a somewhat more distinguished role. Not only does γ control the relative contribution of the two exponential terms in Eq. (3.4), it also enters Eq. (3.4) in a more indirect way through Eqs. (3.5), (3.6), and (3.7); $v_\parallel$, on the other hand, is solely responsible for the period of oscillations in $F(k_\parallel,t)$ (regarding $k_\parallel$ as constant). Thus, for the subsequent analysis of the dynamics in the vicinity of fluid phase transitions, it seems justified to focus on γ and $v_\parallel$. Moreover, since

$$\gamma \equiv \frac{c_{\tau_\parallel}}{c_{As_z}}, \tag{3.12a}$$

$$v_\parallel \equiv -\frac{\gamma}{m}\left(\frac{\partial \tau_\parallel}{\partial \rho}\right)_{N,T,s_z} \tag{3.12b}$$

are purely thermodynamic quantities, we employ a mean-field theory to investigate their behavior as one approaches the spinodal. In Eq. (3.12a), m is the mass of a molecule.

The analysis of γ and $v_\parallel$ departs from the mean-field free energy $\mathcal{F}$ of a confined fluid developed in Ref. [12] where it was shown that

$$\mathcal{F}=-k_BT\left\{N\ln\left[\frac{1-b\rho}{\rho\Lambda^3}\right]+N\right\}+N\Psi(s_z)-Na_p(s_z)\rho. \tag{3.13}$$

In Eq. (3.13), k_B is Boltzmann's constant, ρ is the mean density of the confined fluid, $\Lambda=h/\sqrt{2\pi m k_B T}$ is the thermal de Broglie wavelength (h Planck's constant), $b=2\pi\sigma^3/3$ is the volume excluded to a pair of hard spheres of diameter σ, $\Psi(s_z)$ is the external potential exerted on the confined fluid by two planar, chemically homogeneous substrates separated by a distance s_z, and

$$a_p(s_z)=a_b\left[1-\frac{3\sigma}{4(s_z-2\sigma)}+\frac{1}{8\sigma^3(s_z-2\sigma)^3}\right]\leqslant a_b. \tag{3.14}$$

In Eq. (3.14), $a_b=4\epsilon b$ is the contribution of intermolecular attraction to the bulk free energy where ϵ is the depth of the attractive well. In the limit $s_z\to\infty$, $\Psi(s_z)\to 0$ and $a_p(s_z)\to a_b$ such that Eq. (3.13) reduces to the well-known expression for the free energy of a van der Waals bulk fluid [13].

From Eq. (3.13) and the thermodynamic relation [12]

$$d\mathcal{F}=-\mathcal{S}dT+\mu dN+\tau_\parallel s_z dA+\tau_{zz}Ads_z, \tag{3.15}$$

the equation of state

$$\tau_\parallel=-\frac{\rho^2}{N}\left(\frac{\partial\mathcal{F}}{\partial\rho}\right)_{T,N,s_z}=-\frac{\rho k_BT}{1-b\rho}+a_p(s_z)\rho^2 \tag{3.16}$$

readily emerges. In Eq. (3.15), $\mathcal{S}$ denotes entropy, μ is the chemical potential, $\tau_\parallel\equiv\frac{1}{2}(\tau_{xx}+\tau_{yy})$ and τ_{zz} are diagonal components of the stress tensor, and A is the area of the (planar) solid-fluid interface.

From Eq. (3.13) and the definition,

$$c_{As_z}\equiv\frac{T}{N}\left(\frac{\partial^2\mathcal{F}}{\partial T^2}\right)_{N,A,s_z}=\frac{T}{N}\frac{\partial}{\partial T}\left[\frac{Nk_B}{2}-k_BN\ln\left(\frac{\rho\Lambda^3}{1-b\rho}\right)\right]=\frac{3k_B}{2} \tag{3.17}$$

is obtained which is the ideal-gas expression as expected from mean-field theory. Moreover, thermodynamic consistency requires the expression

$$\gamma=\frac{c_{\tau_\parallel}}{c_{As_z}}=1+\frac{T\alpha_\parallel^2}{\rho c_{As_z}\kappa_\parallel} \tag{3.18}$$

to hold [14]. From Eq. (3.18), the expansion coefficient

$$\alpha_\parallel \equiv -\frac{1}{\rho}\left(\frac{\partial\rho}{\partial T}\right)_{N,\tau_\parallel,s_z} = \frac{k_B(1-b\rho)}{k_BT-2a_{\rm p}(s_z)\rho(1-b\rho)^2} \tag{3.19}$$

and the transverse isothermal compressibility

$$\kappa_\parallel \equiv -\frac{1}{\rho}\left(\frac{\partial\rho}{\partial\tau_\parallel}\right)_{T,N,s_z} = \frac{(1-b\rho)^2}{\rho[k_BT-2a_{\rm p}(s_z)\rho(1-b\rho)^2]} \tag{3.20}$$

are obtained with the aid of Eq. (3.16). Substituting now the far right sides of Eqs. (3.17), (3.19), and (3.20) into Eq. (3.18), we finally obtain

$$\gamma = 1+\frac{2k_BT}{3k_BT-6a_{\rm p}(s_z)\rho(1-b\rho)^2}. \tag{3.21}$$

In the limit of an ideal gas, $\rho\to 0$ and we recover $\gamma^{\rm id}=\frac{5}{3}$ from Eq. (3.21) as we must. This limiting value is also obtained if the ideal gas at arbitrarily high density is perceived as being composed of attractionless ($a_{\rm b}=0$) mathematical points ($\sigma=0$ and therefore $b=0$). Under these assumptions, $\alpha_\parallel^{\rm id}=1/T$, $\kappa_\parallel^{\rm id}=1/\rho k_BT$, and $\gamma^{\rm id}=\frac{5}{3}$ is again recovered from Eq. (3.18) using also Eq. (3.17).

Substituting Eqs. (3.18), (3.19), and (3.20) into Eq. (3.12b), we obtain

$$\begin{aligned} v_\parallel &= \sqrt{\frac{1}{\rho\kappa_\parallel}+\frac{T}{\rho^2 m c_{As_z}}\left(\frac{\alpha_\parallel}{\kappa_\parallel}\right)^2} \\ &= \frac{1}{1-b\rho}\sqrt{k_BT-2a_p(s_z)\rho(1-b\rho)^2+\frac{k_B^2T}{mc_{As_z}}}, \end{aligned} \tag{3.22}$$

which we subject to further analysis in Sec. III D below.

D. Stability of thermodynamic phases

In an open thermodynamic system metastable- or globallystable states are characterized by minima of the grand potential density

$$\omega = \tau_\parallel(\mu,T,A,s_z). \tag{3.23}$$

Equation (3.23) follows from Eq. (3.15) through a Legendre transformation

$$d\Omega \equiv d(\mathcal{F}-\mu N) \tag{3.24}$$

and by noting that $\Omega = As_z\omega$ is a homogeneous function of degree one in A provided all its other natural variables remain constant. Over a certain range of chemical potentials (at fixed T, A, s_z), it may turn out that several minima of ω exist at the same μ. In other words, a range of μ's exists such that $\omega(\mu)$ is a multivalued function, where the lowest value ω^α corresponds to the thermodynamically stable state α whereas the others refer to metastable states. In general, thermodynamics requires the inequalities

$$\left(\frac{\partial\omega^\alpha}{\partial\mu}\right)_{T,A,s_z} = -\rho^\alpha < 0, \tag{3.25a}$$

$$\left(\frac{\partial^2\omega^\alpha}{\partial\mu^2}\right)_{T,A,s_z} = -\rho^\alpha\kappa_\parallel^\alpha < 0, \quad \forall\,\alpha \tag{3.25b}$$

to hold irrespective of T.

Mathematically speaking, at constant T, $\omega(\mu)$ is always a concave [see Eq. (3.25b)], monotonic [see Eq. (3.25a)] function with slope and curvature being determined by the nature of the thermodynamic phase under consideration (i.e., by ρ^α and $\kappa_\parallel^\alpha$). Because of concavity and monotonicity and since, in general, $\rho^\alpha\neq\rho^\beta$ for subcritical thermodynamic states, intersections between ω^α and ω^β exist at which pairs of phases α and β coexist. For a given T, the chemical potential at coexistence $\mu_{\rm x}^{\alpha\beta}$ is obtained by solving the equation

$$\omega^\alpha(\mu_{\rm x}^{\alpha\beta}) = \omega^\beta(\mu_{\rm x}^{\alpha\beta}), \quad T,A,s_z = \text{const.} \tag{3.26}$$

If $\omega^\alpha(\mu_{\rm x}^{\alpha\beta})=\omega^\beta(\mu_{\rm x}^{\alpha\beta})$ is the absolute minimum of the grand-potential density, α and β are thermodynamically stable, coexisting phases.

Suppose, now that the densities of the thermodynamically stable coexisting phases satisfy the inequality

$$\rho^\alpha > \rho^\beta \tag{3.27}$$

such that for $\mu<\mu_{\rm x}^{\alpha\beta}$ the thermodynamically stable phase is α, whereas for $\mu>\mu_{\rm x}^{\alpha\beta}$ this is the case for phase β [see Eq. (3.25a)]. Consequently, α is metastable for $\mu>\mu_{\rm x}^{\alpha\beta}$, whereas this is true for β over the corresponding range $\mu<\mu_{\rm x}^{\alpha\beta}$. Metastable branches end at the stability limit.

Within the scope of mean-field theory, this stability limit is demarcated by a divergence of the isothermal compressibility defined in Eq. (3.20). The divergence occurs at a density $\rho_{\rm s}$ that defines the location of the so-called spinodal at the given temperature T. From Eqs. (3.20) and (3.21), it is straightforward to verify that the divergence of $\kappa_\parallel$ implies a divergence of γ since

$$\kappa_\parallel = \frac{3}{2}\frac{(1-b\rho)^2}{\rho k_BT}(\gamma-1) \tag{3.28}$$

and the factor $(1-b\rho_{\rm s})^2/\rho_{\rm s}k_BT$ remains finite at the spinodal for $T>0$. This is demonstrated in the Appendix where explicit expressions for $\rho_{\rm s}$ are derived [see Eqs. (A11) and (A12)].

Contrary to γ, $v_\parallel$ remains finite and nonzero along the spinodal [15]. This follows from Eqs. (3.19), (3.20), and (A2) which permit us to rewrite Eq. (3.22) as

$$v_\parallel = \frac{1}{1-b\rho_{\rm s}}\sqrt{\frac{k_B^2T}{mc_{As_z}}} = \frac{1}{1-b\rho_{\rm s}}\sqrt{\frac{2}{3}\frac{k_BT}{m}}, \tag{3.29}$$

where the far right side follows from Eq. (3.17). Equation (3.29) shows that at mean-field level and for thermodynamic states along the spinodal, the velocity of sound depends only

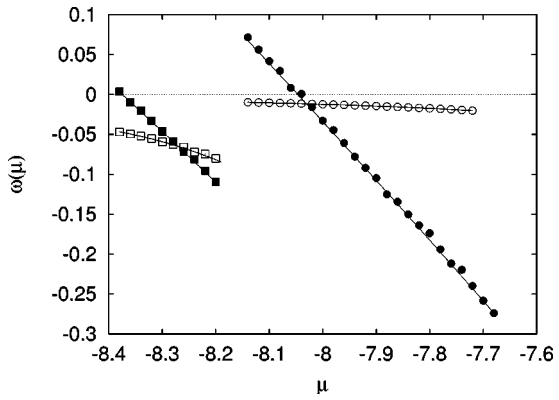

FIG. 3. Grand-potential density $\omega(\mu)$ for $T=0.8$. Symbols refer to bulk gas (○), bulk liquid (●), confined "gas" (□), and confined liquid (■) ($s_z=10$). Solid lines are intended to guide the eye.

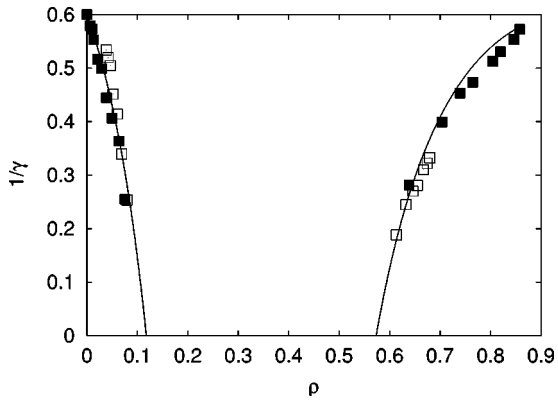

FIG. 4. Ratio $1/\gamma$ of isochoric and isostress heat capacities as a function of density for $T=0.8$ in the bulk. Symbols refer to results obtained by fitting Eq. (3.4) to MD data (□) and to data obtained in Monte Carlo simulations (■) (see text). The solid line represents the fit of Eq. (3.21).

on the volume b, excluded to a pair of hard spheres, but is independent of the attraction between a pair of fluid molecules.

IV. RESULTS

A. Technical details

To locate phase transitions in bulk and confined fluids, we employ grand canonical ensemble Monte Carlo (GCEMC) simulations permitting us to determine $\omega(\mu)$ for various temperatures T from Eq. (3.23) using a molecular expression for $\tau_\parallel$ (see, for example, Eq. (13) in Ref. [16]). Typical results plotted in Fig. 3 illustrate the precision with which a solution of Eq. (3.26) can be obtained numerically. Even though Fig. 3 shows that whereas it is possible in GCEMC to simulate states well inside the metastable regime of either gas or liquid, it is generally not possible to go directly to the stability limit (i.e., the spinodal). The reason is that the local minimum of ω at the equilibrium mean density becomes rather shallow, and density fluctuations increase simultaneously as one approaches the spinodal. However, the shallower the minimum of ω, the larger is the probability that a sufficiently large density fluctuation may eventually arises which may then carry the system over the grand-potential barrier separating the metastable state from the globally stable one at a lower ω. To locate the spinodal, we therefore turn to MD simulations in the microcanonical ensemble using as input the mean number of fluid molecules obtained from GCEMC for a given μ and T, and states off the spinodal. This assumes implicitly that for the typical system sizes used in this study, the principle of equivalence of statistical physical ensembles applies [17]. The MD simulations are performed according to the conditions summarized in Ref. [1].

The subsequent analysis of $M(k_\parallel,t)$ to obtain γ and $v_\parallel$, which are the quantities of key interest in the present context, then proceeds as follows. From Eqs. (3.10a) and (3.11), it is clear that the scaling laws

$$M_0(k_\parallel)\propto k_\parallel^2, \tag{4.1a}$$

$$x''^2\propto k_\parallel^2 \tag{4.1b}$$

should hold in the hydrodynamic regime (see also Figs. 2, 3, 5 and Secs. IV B, IV C of Ref. [1]). Let m_1 and m_2 be constants of proportionality in the respective scaling laws for M_0 and x'' [see Eqs. (4.1)] which are determined as slopes of linear least squares fits. It is then easy to verify from Eqs. (3.10a) and (3.10c) that

$$\gamma=1+\frac{m_1}{m_2}, \tag{4.2a}$$

$$v_\parallel=\sqrt{m_1+m_2} \tag{4.2b}$$

provide a means to calculate γ and $v_\parallel$, simultaneously.

B. Locating the bulk spinodal

In Fig. 4, we plot $1/\gamma$ as a function of ρ and $T=0.8$. Two branches at low(er) and high(er) densities are clearly discernible. As ρ increases in the low-density regime, $1/\gamma$ decreases, whereas in the high-density regime it rises with ρ. To check the accuracy of γ obtained from the procedure detailed in Sec. IV A, we compare with results from Monte Carlo simulations in the mixed isostress-isostrain ensemble introduced in Ref. [14]. In the mixed isostress-isostrain ensemble (fixed N, T, $\tau_\parallel$, s_z), the molar isostress heat capacity is

$$c_{\tau_\parallel}=\frac{3}{2}k_B+\frac{1}{Nk_BT^2}[\langle\tilde{\mathcal{H}}^2\rangle-\langle\tilde{\mathcal{H}}\rangle^2], \tag{4.3}$$

where the (configurational part of the average) enthalpy is given by

$$\langle\tilde{\mathcal{H}}\rangle=-\tau_\parallel\langle A\rangle s_z+\langle U\rangle \tag{4.4}$$

and $\langle U\rangle$ is the (average) configurational energy [14]. In the canonical ensemble (fixed N, T, A, s_z), the (molar) isochoric heat capacity is given by

$$c_{As_z}=\frac{3}{2}k_B+\frac{1}{Nk_BT^2}[\langle U^2\rangle-\langle U\rangle^2]. \tag{4.5}$$

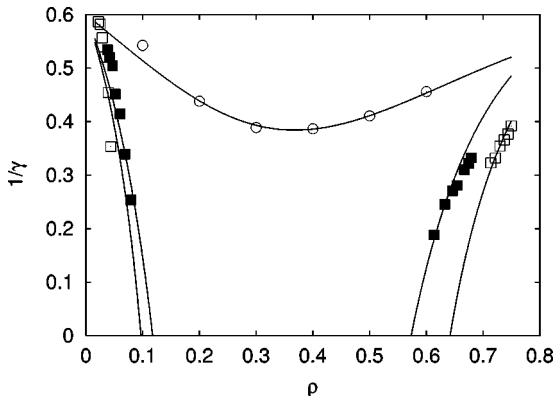

FIG. 5. As Fig. 4, but for various temperatures $T=0.7$ (□), $T=0.8$ (■), and $T=1.5$ (○). Solid lines represent fits of Eq. (3.21).

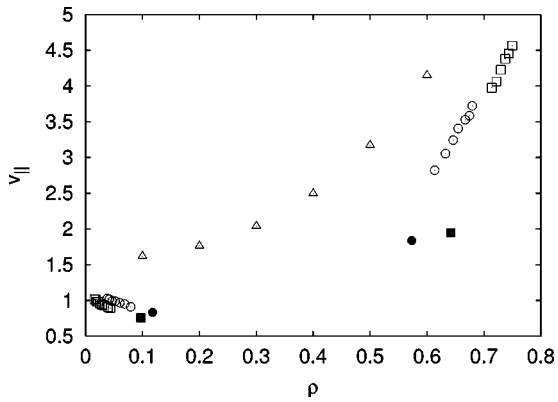

FIG. 6. As Fig. 5, but for $v_\parallel$; $T=0.7$ (□), $T=0.8$ (○), and $T=1.5$ (△) calculated from Eq. (4.2b). Filled symbols represent values at the spinodal calculated from Eq. (3.29); $T=0.7$ (■) and $T=0.8$ (●).

Angular brackets indicate averages in the respective ensemble. Thus, Eqs. (3.18) and (4.3)–(4.5) offer a possibility to calculate γ from a sequence of Monte Carlo simulations in a generalized isostress-isostrain and the canonical ensembles. Plots in Fig. 4 indicate not only the excellent mutual agreement between both data sets but also the high quality of the fit provided by Eq. (3.21). From the fit, we estimate $\rho_s^{ld} \simeq 0.12$ on the low(er)-density (i.e., gas) side, whereas on the high(er)–density (i.e., liquid) side $\rho_s^{hd} \simeq 0.58$. Note that in the limit $\rho \to 0$, the ideal-gas value $\gamma^{id}=\frac{5}{3}$ is recovered from the plot in Fig. 4 as expected from Eq. (3.21).

If the temperature increases, one expects the densities of the gas and liquid branches of the spinodal to become more and more alike as one can verify from Eq. (A7b) which implies

$$\lim_{T\to T_{cb}^-} (\rho_s^g - \rho_s^l) \propto \lim_{T\to T_{cb}^-} \sin\frac{\varphi(T)}{3} = 0. \tag{4.6}$$

In Eq. (4.6), T_{cb} is the bulk critical temperature defined in Eq. (A9). Plots in Fig. 5 for $T=0.7$ and 0.8 confirm Eq. (4.6), because $\sin[\varphi(T)/3]$ decreases monotonically with increasing T [see Eq. (A13)].

From Fig. 5, one also notices that for a sufficiently high temperature $T=1.5$, the divergence of γ apparently disappears, that is, $1/\gamma$ exhibits a minimum at some density rather than going to zero. From Eq. (3.21), it is straightforward to verify that at mean-field level

$$\left(\frac{\partial \gamma^{-1}}{\partial \rho}\right)_T = -\frac{1}{\gamma^2}\left(\frac{\partial \gamma}{\partial \rho}\right)_T = \frac{12 a_p(s_z) k_B T (1-b\rho)(3b\rho-1)}{[5k_BT - 6a_p(s_z)\rho(1-b\rho)^2]^2} \overset{!}{=} 0 \tag{4.7}$$

is the necessary condition for an extremum of $1/\gamma$ to exist. Formally, Eq. (4.7) has solution $\rho=1/b$, which is physically not sensible since it corresponds to an infinite value of $\tau_\parallel$ in Eq. (3.16), and $\rho=\rho_c=1/3b$ corresponding to the critical density. From the plot in Fig. 5, a rough estimate of $\rho_c \simeq 0.37$ is obtained which is only 14% higher than the much more accurate result $\rho_c=0.3197$ of Wilding [18] who used a sophisticated weigthed-histogram Monte Carlo technique. It should be noted, however, that while also using a potential cutoff $r_c=2.5$, Wilding left his intermolecular potential unshifted, that is, in his expression for u_{ff} the terms $u_{LJ}(r_c)$ as well as $u'_{LJ}(r_c)(r_c-r)$ were absent. According to Smit [19], this should have only a marginal effect on ρ_c but a significant impact on the critical temperature. However, we note that the point of our work is not to estimate with high accuracy the critical-point location for which a mean-field theory would be inadequate anyhow.

As already emphasized in Sec. III D, $v_\parallel$ should remain finite and nonzero at the spinodal [15]. Plots in Fig. 6 support this notion. It seems particularly noteworthy that data points off the spinodal, which were obtained through the procedure detailed in Sec. IV A [see Eq. (4.2b)], are fully consistent with the ones located directly on the spinodal, calculated independently from Eq. (3.29), where b from the fit to the corresponding data for $1/\gamma$ plotted in Fig. 5 was used. As expected, $v_\parallel$ changes discontinuously at the spinodal, whereas it varies continuously and monotonically for supercritical thermodynamic states as one can infer also from the plots in Fig. 6.

C. Confinement effects

If the fluid is now confined to a slit pore of $s_z=10$, the scenario illustrated by Figs. 4 and 5 changes in a significant way. This can be seen from Fig. 7 where we plot $1/\gamma$ as a function of ρ for the bulk and for the confined system at the same temperature $T=0.7$. From the figure, one notices that apart from a shift in density, the high-density branch ($\rho > 0.6$) remains qualitatively unaffected by confinement. On the low-density side, however, $1/\gamma$ for the confined fluid does not immediately go to zero but exhibits a minimum apparently not accounted for by the mean-field equation (3.21). Even though $1/\gamma$ vanishes for $\rho_s^{ld} \simeq 0.4$, it does not go monotonically to the ideal-gas value as predicted by the mean-field expression, Eq. (4.7), which implies $(\partial \gamma^{-1}/\partial \rho)_T < 0$ for all densities $\rho \leqslant \rho_s^{ld}$ [see Eq. (A11)]. However, numerically $\gamma^{id}=\frac{5}{3}$ is recovered in the limit $\rho \to 0$ as it must [see Eq. (3.21)].

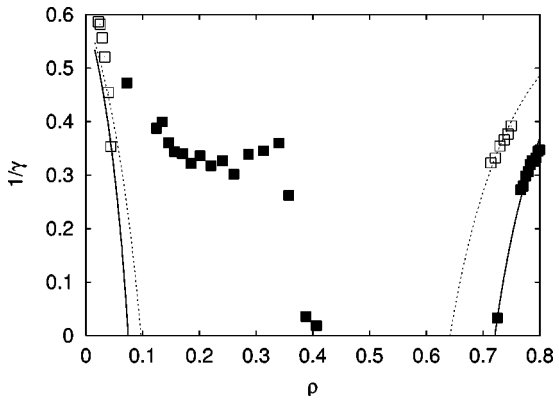

FIG. 7. As Fig. 4, but for $T=0.7$ in the bulk (□) and a confined fluid ($s_z=10$) (■). The dashed line represents a fit of Eq. (3.21) to all bulk data points. The solid line is obtained by a fit of Eq. (3.21) only to data points along the high-density branch of the confined fluid ($\rho>0.7$).

To understand the origin of this minimum, we analyze in Fig. 8 the local density

$$\rho(z)\equiv\frac{\langle N(z)\rangle}{s_x s_y \delta z}, \tag{4.8}$$

where $N(z)$ is the number of molecules located at $z\pm\delta z/2$ ($\delta z=0.05$) in a given configuration and $\langle\cdots\rangle$ indicates an average in the grand canonical ensemble. Over the density range $0.06\lesssim\rho\lesssim0.34$, where $1/\gamma$ exhibits minimum parallel plots in Fig. 8 show that a thin film of fluid is adsorbed on each substrate which thickens as ρ (i.e., μ) increases. This film consists of individual layers of molecules as reflected by the nonmonotonic dependence of $\rho(z)$ on z, where maxima correspond to the center of mass of each layer. On account of the diminishing fluid-substrate attraction, these layers become increasingly less pronounced as one departs from the substrate surface. However, $\rho(z)$ assumes rather low (i.e., gaslike) values around the center of the slit pore reflecting the low probability of finding fluid molecules. As μ increases, capillary condensation eventually sets in and the gaslike inner part of the pore is then occupied by high-density fluid. For the present choice of system parameters, we did not observe prewetting but rather a steady and continuous increase in the thickness of the adsorbed film (see also Sec. V). The approach of the stability limit of the adsorbed film is again reflected by $1/\gamma$ going to zero at the spinodal $\rho_s^{ld}\simeq0.4$, which is now much higher than for the corresponding bulk system (see Fig. 7).

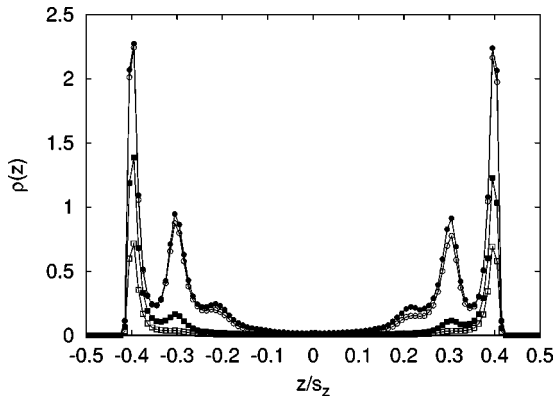

FIG. 8. Local density $\rho(z)$ as a function of position z between lower ($z/s_z=-0.5$) and upper ($z/s_z=+0.5$) substrates; (□) $\rho=0.06$, (■) $\rho=0.12$, (○) $\rho=0.31$, and (●) $\rho=0.34$ (see Fig. 7).

Since the adsorbed film is highly inhomogeneous, it seems not surprising that the associated change in $1/\gamma$ cannot be accounted for by the simple mean-field theory summarized in Sec. III C which explicitly assumes a *homogeneous* confined phase [12]. Once the fluid underwent capillary condensation, however, the present pore width $s_z=10$ is large enough for a homogeneous midsection (centered on $z=0$) of the confined fluid to exist. Then, the mean-field treatment becomes more appropriate and consequently data points on the liquid side of the spinodal ($\rho>0.6$, see Fig. 7) are represented properly by Eq. (3.21) (see Fig. 7).

The divergence of γ at the spinodal has consequences for the decorrelation of density modes reflected by the decay of $F(k_\parallel,t)$ as time passes. Noticing from Eqs. (3.5)–(3.7) that

$$\lim_{\gamma\to\infty} D_T=0, \tag{4.9a}$$

$$\lim_{\gamma\to\infty}\Gamma=\frac{1}{2}(a+b_\parallel), \tag{4.9b}$$

$$\lim_{\gamma\to\infty} d(k_\parallel)=(3a+b_\parallel)\frac{k_\parallel}{3v_\parallel} \tag{4.9c}$$

and one readily concludes from Eq. (3.4) that

$$\lim_{\gamma\to\infty} F(k_\parallel,t)=1,\quad \forall\, t, \tag{4.10}$$

where we implicitly assume a, $b_\parallel$, and $v_\parallel$ to remain finite at the spinodal. Plots in Fig. 9 corroborate this notion. Hence, as one approaches the stability limit of either bulk or confined phases, there is a significant lack of decorrelation in the collective dynamics. Our results would suggest that decorrelation is completely absent for thermodynamic states located *directly* on the spinodal. Intuitively, it might be easier to grasp this effect in terms of the memory kernel $M(k_\parallel,t)$. For example, taking the Laplace transform of Volterra's equation [see Eq. (3.8)] and noticing that the Laplace transform of $F(k_\parallel,t)$ in Eq. (4.10) is $1/s$, one has $M(k_\parallel,s)=0$. A trivial backtransformation to the time domain leads to $M(k_\parallel,t)=0$. In other words, collective dynamic modes for states directly on the spinodal completely lack any ''memory'' of their past.

V. SUMMARY AND CONCLUSIONS

In this work, we are concerned with extending the analysis of $F(k_\parallel,t)$ described in Ref. [1] to thermodynamic states in the vicinity of a fluid phase transition. Our results show that as one penetrates into the metastable regime of fluid phases, decorrelation of propagating collective (density)

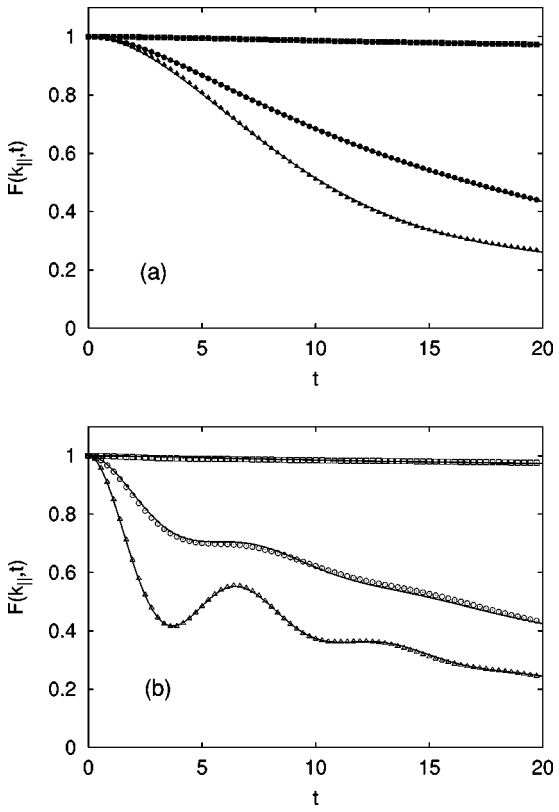

FIG. 9. As Fig. 1(a), but for confined fluids ($s_z=10$) at various densities and $k_\parallel=0.25$; (a) $\rho=0.1$ (▲), $\rho=0.2$ (●), $\rho=0.4$ (■); (b) $\rho=0.79$ (△), $\rho=0.75$ (○), $\rho=0.72$ (□) (see also Fig. 7). Solid lines are fits of Eq. (3.4) intended to guide the eye.

modes becomes increasingly slower; as the fluid reaches its stability limit (i.e., at the locus of the spinodal), a decorrelation of these modes is practically absent. This becomes apparent from $F(k_\parallel,t)$ that remains nearly unity for all times.

Within a mean-field treatment, the concept of a spinodal is associated with a divergence of the isothermal compressibility. Since $\kappa_\parallel$ is directly proportional to the ratio of heat capacities γ, which is one of the parameters governing the shape of $F(k_\parallel,t)$ in the hydrodynamic regime, the increasingly slow decay of $F(k_\parallel,t)$ with time can be ascribed to a divergence of γ at the spinodal. Obviously, γ can diverge only for *sub*critical temperatures. For *super*critical temperatures, on the other hand, γ passes through a maximum ($1/\gamma$ passes through a minimum) at the critical density of the fluid. Thus, for supercritical states, the $F(k_\parallel,t)$ remains a damped oscillatory function of time. Only quantitative changes in amplitude and damping characteristics of these oscillations reflect changes in the thermodynamic state.

Unfortunately, the mean-field theory is only of limited use as far as confined fluids are concerned. It describes correctly the divergence of γ as one approaches the spinodal from the high(er)-density (i.e., liquid) side of the phase diagram, but fails to account for the more complex variation of γ on the low(er)-density side of the phase diagram. The more complex dependence of γ for low(er)-density states is a result of the growth of fluid layers on each substrate prior to capillary condensation, whereupon γ diverges in a qualitatively similar fashion as observed before in the bulk. Since the mean-field theory employed here is based upon the explicit assumption that the pore phase is homogeneous in all three spatial dimensions, it seems not surprising that it cannot account for effects associated with structural changes in a highly inhomogeneous confined phase.

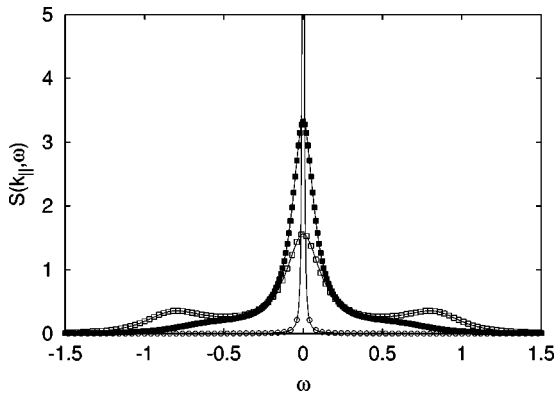

FIG. 10. Dynamic structure factor $S(k_\parallel,\omega)$ as a function of frequency ω for confined fluid ($T=0.7$, $s_z=10$, $k_\parallel=0.25$). Curves are shown for densities $\rho=0.79$ (□), 0.75 (■), and 0.72 (○) and lines are fits of Eq. (4.11) of Ref. [1] intended to guide the eye (see also Fig. 9).

One may also speculate that if multilayer adsorption is accompanied by a prewetting transition that γ may show two divergences: one associated with the coexistence of microscopically thin films of different thicknesses (i.e., the prewetting transition) and another one associated with the condensation of such a film (i.e., capillary condensation). Since the present system did not exhibit a prewetting transition, we are currently extending our study to a case where it seems more likely that such a prewetting transition may, in fact, occur.

Our study may also have important repercussions for scattering experiments in the vicinity of a phase transition in confined fluids. For thermodynamically stable states, the dynamic structure factor $S(k_\parallel,\omega)$, which is measured in light scattering experiments, consists of three lines, namely, the Rayleigh peak centered at the frequency $\omega=0$ and two Brillouin peaks shifted by $\Delta\omega=\pm v_\parallel k_\parallel$ ($k_\parallel\to 0$) relative to the Rayleigh line. Since $S(k_\parallel,\omega)$ is related to $F(k_\parallel,t)$ through a Laplace transformation, it is clear that as one approaches the spinodal [where $F(k_\parallel,t)=1$] the set of Brillouin and Rayleigh lines should be replaced by a single line such that directly at the spinodal $S(k_\parallel,\omega)=\delta(\omega)$. This change in $S(k_\parallel,\omega)$, illustrated by the plots in Fig. 10 for liquidlike states of the confined fluid, should be detectable in scattering experiments on fluids confined to ordered porous matrices such as MCM-41 or SBA-15 types of materials, and should therefore provide experimental insight into the collective dynamics and its relation to the phase behavior of confined and bulk fluids.

ACKNOWLEDGMENTS

We are grateful to the Sonderforschungsbereich 448 ''Mesoskopisch strukturierte Verbundsysteme'' for financial support.

APPENDIX: LOCATION OF THE SPINODAL

At mean-field level, thermodynamic states along the spinodal are characterized by an infinitely large isothermal compressibility, that is, they satisfy the equation

$$\frac{1}{\kappa_{\parallel}(\rho_s)}=0, \tag{A1}$$

which is equivalent to [see Eq. (3.20)]

$$k_BT-2a_p(s_z)\rho_s(1-b\rho_s)^2=0. \tag{A2}$$

The zeros of this cubic polynomial can be found analytically. Therefore, we introduce the transformation

$$\rho_s\rightarrow\tilde{\rho}_s=\rho_s-\frac{2}{3b}, \tag{A3}$$

which permits us to rewrite Eq. (A2) as

$$\tilde{\rho}_s^3-\frac{1}{3b^2}\tilde{\rho}_s+\frac{2}{27b^3}-\frac{k_BT}{2a_p(s_z)b}=0. \tag{A4}$$

Equation (A4) is of the general form $\tilde{\rho}_s^3+p\tilde{\rho}_s+q=0$, where

$$p=-\frac{1}{3b^2}, \tag{A5a}$$

$$q=\frac{2}{27b^3}-\frac{k_BT}{2a_p(s_z)b}. \tag{A5b}$$

Hence, Eq. (A4) is amenable to an analytic solution using the Cardanic formulas [20]. With these identifications, the three real solutions of Eq. (A4) can be cast compactly as

$$\tilde{\rho}_s^{[k]}(T)=2\sqrt[3]{\chi}\cos\left[\frac{\varphi(T)+2(k-1)\pi}{3}\right],\quad k=1,2,3, \tag{A6}$$

where

$$\chi\equiv\sqrt{-\frac{p^3}{27}}=\frac{1}{27b^3}, \tag{A7a}$$

$$\varphi(T)\equiv\arccos\left(-\frac{q}{2\chi}\right)=\arccos\left(\frac{2T-T_{cp}(s_z)}{T_{cp}(s_z)}\right), \tag{A7b}$$

and Eqs. (A5) have also been used. In Eq. (A7b), we have also utilized the fact that the pore critical temperature $T_{cp}(s_z)$ is defined as [12]

$$k_BT_{cp}(s_z)=\frac{8a_p(s_z)}{27b}. \tag{A8}$$

Because of Eq. (3.14),

$$\lim_{s_z\rightarrow\infty}T_{cp}(s_z)=T_{cb}, \tag{A9}$$

where T_{cb} is the critical temperature in the bulk. Moreover, introducing the critical density ρ_c (of bulk and confined fluid) through [12]

$$\rho_c=\frac{1}{3b} \tag{A10}$$

and reverting the transformation [see Eq. (A3)] one can easily verify that the density of states along the low-density (ld) branch of the spinodal is given by

$$\rho_s^{ld}(T)\equiv\rho_s^{[2]}(T)=2\rho_c\left[1+\cos\left(\frac{\varphi(T)+2\pi}{3}\right)\right], \tag{A11}$$

whereas the density along the high-density branch is obtained from

$$\rho_s^{hd}(T)\equiv\rho_s^{[3]}(T)=2\rho_c\left[1+\cos\left(\frac{\varphi(T)+4\pi}{3}\right)\right]. \tag{A12}$$

The fact that Eqs. (A11) and (A12) describe low- and high-density branches of the spinodal, respectively, can be verified by realizing that the spinodal is defined only for temperatures in the range $0\leqslant T\leqslant T_{cp}(s_z)$ so that $\varphi(T)$ is defined over the range

$$\pi\geqslant\varphi(T)\geqslant 0 \tag{A13}$$

and therefore

$$0\leqslant\rho_s^{ld}(T)\leqslant\rho_{cp}, \tag{A14a}$$

$$3\rho_{cp}>\rho_s^{hd}(T)\geqslant\rho_{cp}. \tag{A14b}$$

The solution for $k=1$ in Eq. (A6) is unphysical because it gives rise to a density exceeding $3\rho_{cp}$ over the range of values $\varphi(T)$ can attain. For these densities, $\tau_{\parallel}$ in Eq. (3.16) is positive indicating that the fluid is mechanically unstable.

In Sec. III C, it was also argued that the inequality

$$\frac{(1-b\rho_s)^2}{\rho_sk_BT}<\infty,\quad T>0 \tag{A15}$$

holds such that a divergence of $\kappa_{\parallel}$ directly implies a divergence of γ. Replacing in the inequality (A15), ρ_s by either ρ_s^{ld} or ρ_s^{hd} from Eqs. (A11) or (A12), respectively, it is clear that the numerator of the resulting expression remains finite since the density on the spinodal is finite. Moreover, it can easily be verified that the denominator contains the factor

$$T\left[1+\cos\left(\frac{\varphi(T)+n\pi}{3}\right)\right]\geqslant 0, \tag{A16}$$

where $n=2$ for ρ_s^{ld} and $n=4$ for ρ_s^{hd}, and the equal sign holds only for $T=0$. Thus, for $T>0$, the left side of the inequality (A15) is indeed finite and positive as it must [see Eq. (3.28)].

[1] F. Porcheron and M. Schoen, Phys. Rev. E **66**, 041205 (2002).
[2] M. Schoen, R. Vogelsang, and C. Hoheisel, Mol. Phys. **57**, 445 (1986).
[3] R. D. Mountain, Rev. Mod. Phys. **38**, 205 (1966).
[4] D. McIntyre and J. V. Sengers, in *Physics of Simple Liquids*, edited by H. N. V. Temperley, J. S. Rowlinson, and G. S. Rushbrooke (North-Holland, Amsterdam, 1968), p. 480.
[5] M. P. Allen and D. J. Tildesley, *Computer Simulation of Liquids* (Academic, London, 1987).
[6] W. Brown, *Dynamic Light Scattering* (Clarendon, Oxford, 1993).
[7] B. J. Berne and R. Pecora, *Dynamic Light Scattering* (Wiley, New York, 1976).
[8] C.H. de Novion, Radiat. Phys. Chem. **51**, 637 (1998).
[9] Because of a typographical error $\rho_s\sigma^2=1.0$ in Ref. [1] should be replaced by the value 0.79 given in Sec. II.
[10] J. P. Hansen and I. R. McDonald, *Theory of Simple Liquids*, 2nd ed. (Academic, London, 1986).
[11] B. J. Berne and G. D. Harp, Adv. Chem. Phys. **17**, 63 (1970).
[12] M. Schoen and D. J. Diestler, J. Chem. Phys. **109**, 5596 (1998).
[13] R. Balian, *From Microphysics to Macrophysics* (Springer-Verlag, Berlin, 1991), Vol. I, p. 400.
[14] M. Schoen, Physica A **270**, 353 (1999).
[15] F. Kohler, *The Liquid State* (Verlag Chemie, Weinheim, 1972).
[16] S. Sacquin, M. Schoen, and A. H. Fuchs, Mol. Phys. **100**, 2971 (2002).
[17] T. L. Hill, *Statistical Mechanics, Principles and Selected Applications* (Dover, Mineola, 1987).
[18] N. Wilding, Phys. Rev. E **52**, 602 (1995).
[19] B. Smit, J. Chem. Phys. **96**, 8639 (1992).
[20] I. N. Bronstein and K. A. Semendjajew, *Taschenbuch der Mathematik*, edited by G. Grosche, V. Ziegler, and D. Ziegler (Teubner Verlagsgesellschaft, Stuttgart, 1991), p. 131.